

---

# Direction of Arrival Estimation of Wide-band Signals with Planar Microphone Arrays

---

A PREPRINT

Rudolf W Byker and Thomas R Niesler

Department of Electrical and Electronic Engineering, Stellenbosch University, South Africa

March 14, 2022

## ABSTRACT

An approach to the estimation of the Direction of Arrival (DOA) of wide-band signals with a planar microphone array is presented. Our algorithm estimates an unambiguous DOA using a single planar array in which the microphones are placed fairly close together and the sound source is expected to be in the far field. The algorithm uses the ambiguous DOA estimates obtained from microphone pairs in the array to determine an unambiguous DOA estimate for the array as a whole. The required pair-wise DOAs may be calculated using Time Delay Estimations (TDEs), which may in turn be calculated using cross-correlation, making the algorithm suitable for wide-band signals. No a priori knowledge of the true Sound Source Location (SSL) is required. Simulations show that the algorithm is robust against noise in the input data. An average ratio of approximately 3:1 exists between the input DOA errors and the output DOA error. Field tests with a moving sound source provided DOA estimates with standard deviations between  $20.4^\circ$  and  $15.2^\circ$ .

**Keywords** wideband direction of arrival estimation, planar microphone array, elephant rumble sounds

## 1 INTRODUCTION

The Direction of Arrival (DOA) estimate provided by a linear microphone array is always ambiguous, because there is no change in the measured signals when the Sound Source Location (SSL) is reflected along the array axis. Other non-trivial ambiguities may also exist [1].

A triangulation algorithm which removes these ambiguities when three or more linear microphone arrays are present has been proposed by Ottoy and De Strycker [2]. We extend this approach to allow the estimation of an unambiguous DOA for a single non-linear planar microphone array. We assume that the microphones comprising the array are closely spaced relative to the expected distance to the sound source (i.e. the sound source is situated in the far field). In this situation, the Time Delay Estimate (TDE) obtained from any pair of microphones in the array provides an ambiguous DOA estimate. With  $M$  microphones, there are  $N = \binom{M}{2}$  possible pairs, providing  $2^N$  possible DOA solutions. We define an error function that can be minimised to determine the best solution, thereby eliminating the DOA ambiguities of the individual microphone pairs.

Although the underlying mathematical derivations are similar, our algorithm differs from Ottoy and De Strycker's method in the following ways:

1. Ottoy and De Strycker estimate a SSL, while we estimate a DOA.
2. The method presented by Ottoy and De Strycker requires three or more linear arrays spaced far apart, with the SSL residing in the far field with respect to the elements within each array, but in the near field with respect to the arrays themselves. We use a single non-linear, planar array, where the SSL is in the far field with respect to the elements within the array. Of course, triangulation may still be performed after our method has been applied to two or more such arrays.

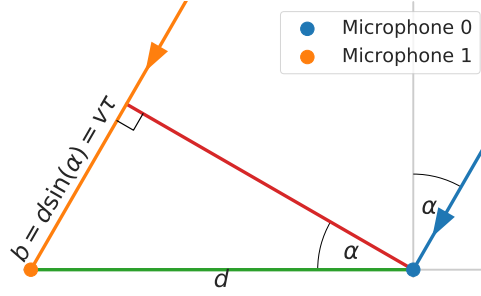


Figure 1: When the sound source is in the far field with respect to the microphone pair (i.e. the distance to the sound source is much larger than  $d$ ), the vectors from the SSL to the microphones may be considered parallel.

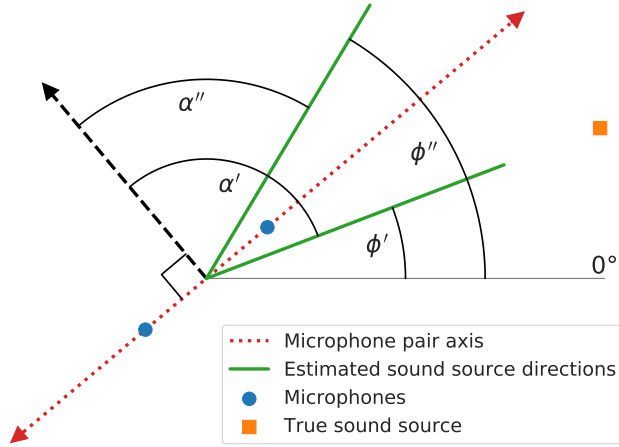


Figure 2: Since sound sources with DOAs  $\alpha'$  and  $\alpha''$  lead to the same TDOA for the microphone pair, there is a DOA ambiguity. The DOAs relative to the coordinate system of the microphone pair are indicated by  $\alpha'$  and  $\alpha''$ . The DOAs relative to the polar coordinate system are indicated by  $\phi'$  and  $\phi''$ .

Both methods aim to resolve the DOA ambiguities inherent to linear arrays.

In §2 we review the existing algorithm presented by Ottoy and De Strycker, and in §3 we present our proposed method. Simulations (§4) and tests (§5) are performed to verify the algorithm.

## 2 BACKGROUND

### 2.1 DOA Estimation with a single microphone pair

When two closely-spaced microphones measure the same far-field signal, the vectors from the SSL to each microphone may be regarded as parallel, as shown in Figure 1. The Time Difference of Arrival (TDOA) between the microphones relates to the DOA as indicated by Equation 1 where  $\alpha$  is the DOA of the sound source,  $v$  is the speed of sound,  $d$  is the microphone pair distance, and  $\tau$  is the TDOA estimate [3, 4]. The TDOA may be estimated using any known method, such as cross correlation.

$$\alpha = \arcsin\left(\frac{\tau v}{d}\right) \quad (1)$$

With two microphones, the DOA always has an alias. As demonstrated in Figure 2, sound sources with DOAs  $\alpha'$  and  $\alpha''$  have the same TDOA, and therefore cannot be distinguished. The same ambiguity exists in any linear microphone array [1].

Since each microphone pair has its own coordinate system, the rest of this paper will use the DOA estimates relative to the polar coordinate system ( $\phi$ ) instead of the DOA estimates relative to the coordinate systems of the individual microphone pairs ( $\alpha$ ), as illustrated in Figure 2.

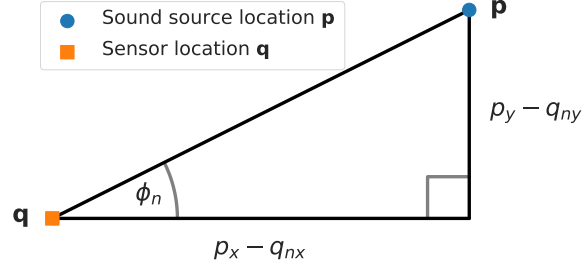


Figure 3: The DOA estimate  $\phi_n$  is related trigonometrically to the sensor location  $\mathbf{q}_n = [q_{nx}, q_{ny}]$  and the SSL  $\mathbf{p} = [p_x, p_y]$ .

## 2.2 Triangulation with multiple DOA estimates

When multiple unambiguous DOA estimates are available from two or more different sensor locations to the same sound source, triangulation may be performed to estimate the SSL [2, 5]. A DOA estimate  $\phi_n$ , its sensor location  $\mathbf{q}_n = [q_{nx}, q_{ny}]$  and the SSL  $\mathbf{p} = [p_x, p_y]$  are related by Equation 2 as depicted in Figure 3.

$$\tan(\phi_n) = \frac{p_y - q_{ny}}{p_x - q_{nx}} \quad (2)$$

Since  $p_x$  and  $p_y$  are unknown, two sensors and two such equations are needed to solve for the SSL. With more than two sensors, an over-determined system of linear equations is produced, as shown in Equation 3, which may be solved using the least squares method [2, 6, 7].

$$\begin{bmatrix} -\tan(\phi_1) & 1 \\ -\tan(\phi_2) & 1 \\ \vdots & 1 \\ -\tan(\phi_N) & 1 \end{bmatrix} \begin{bmatrix} p_x \\ p_y \end{bmatrix} = \begin{bmatrix} q_{1,y} - q_{1,x} \tan(\phi_1) \\ q_{2,y} - q_{2,x} \tan(\phi_2) \\ \vdots \\ q_{N,y} - q_{N,x} \tan(\phi_N) \end{bmatrix} \quad (3)$$

## 2.3 Ottoy and De Strycker's method for solving DOA ambiguities

An algorithm to overcome the DOA ambiguity while performing triangulation was previously presented by Ottoy and de Strycker [2]. We briefly review this algorithm here.

Each sensor location  $\mathbf{q}_n = [q_{nx}, q_{ny}]$  is referred to as a 'node'. This may be a microphone pair, linear microphone array, or any other sensor providing an ambiguous DOA estimate  $\phi_n$ . Each estimate may take on one of two values, which we call  $\phi'_n$  and  $\phi''_n$ . If there are  $N$  nodes, then there are  $I = 2^N$  ways to interpret the set of estimates  $\{\phi_1, \phi_2, \dots, \phi_N\}$ . For each interpretation  $\{\phi_{1,i}, \phi_{2,i}, \dots, \phi_{N,i}\}$ , with  $i \in \{1, 2, \dots, I\}$ , Equation 3 is solved to obtain an estimated SSL  $\hat{\mathbf{p}}_i = [\hat{p}_{x,i}, \hat{p}_{y,i}]$ , after which the angle from  $\mathbf{q}_n$  to  $\hat{\mathbf{p}}_i$  for each  $n$  is given by Equation 4.

$$\hat{\phi}_{n,i} = \arctan\left(\frac{\hat{p}_{y,i} - q_{ny}}{\hat{p}_{x,i} - q_{nx}}\right) \quad (4)$$

The absolute error associated with any one interpretation  $\{\phi_{1,i}, \phi_{2,i}, \dots, \phi_{N,i}\}$  is defined by Equation 5. This is the sum of the absolute differences between the DOA estimate given by each array and the angle between that array and the estimated SSL.

$$\phi_{err,i} = \sum_{n=1}^N |\phi_{n,i} - \hat{\phi}_{n,i}| \quad (5)$$

The interpretation where  $i = \arg \min_i \{\phi_{err,i}\}$  is used to calculate the final SSL.

## 3 EXTENSION TO A SINGLE PLANAR ARRAY

The algorithm presented by Ottoy and De Strycker works well for situations in which:

1. the microphones within each array are closely spaced in relation to the expected SSLs, so that the sound sources are in the far field in relation to the individual microphones, and

2. the arrays themselves are spaced far apart, so that the sound sources are in the near field with respect to the arrays.

The algorithm can be extended to perform a DOA estimation for a single planar array for which the sound source is in the far field, by 1. redefining the  $N$  ‘nodes’ to be the possible combinations of microphone pairs within the planar array, and 2. redefining the error function. We will accomplish this in the following paragraphs.

### 3.1 Pair-wise DOA estimation

We now regard each possible pair of microphones in the planar array as a distinct two-element linear array, and refer to this as a ‘node’. For an array with  $M$  microphones, there are  $N = \binom{M}{2}$  possible nodes. As before (see Figure 2), each node provides two possible solutions,  $\phi_n'$  and  $\phi_n''$ , and the correct solution is one of  $I = 2^N$  possible interpretations  $\{\phi_{1,i}, \phi_{2,i}, \dots, \phi_{N,i}\}$  of the set  $\{\phi_1, \phi_2, \dots, \phi_N\}$ , with  $i \in \{1, 2, \dots, I\}$ .

### 3.2 Error function

Assuming that the sound source is in the far field, we may consider all microphone pairs to be at the same position. Hence we can consider the correct DOA solution to be the one for which the DOA estimate of all pairs agree. To find the solution that is closest to this ideal, a new error function is defined.

The values in each set  $\{\phi_{1,i}, \phi_{2,i}, \dots, \phi_{N,i}\}$  are discrete points in a continuous space. To find the mode of such a dataset, Kernel Density Estimation (KDE) may be performed. Since the domain of the data is wrapped, the von Mises kernel, which is an approximation of the wrapped normal distribution, is appropriate [8, 9, 10]. The von Mises kernel is given by Equation 6, where  $I_0$  is the modified zero’th order Bessel function,  $\mu$  is the mean and  $\kappa$  is the concentration, which determines the width of the kernel. Small values of  $\kappa$  correspond to wide kernels, and vice versa.

$$f_{\text{kernel}}(\phi|\mu, \kappa) = \frac{\exp(\kappa \cos(\phi - \mu))}{2\pi I_0(\kappa)} \quad (6)$$

The KDE of interpretation  $i$  is given by Equation 7.

$$g_i(\phi|\kappa) = \frac{1}{N} \sum_{n=1}^N f_{\text{kernel}}(\phi|\mu = \phi_{n,i}, \kappa) \quad (7)$$

We define the ‘concensus’ DOA estimate for interpretation  $i$  as the mode of the KDE, as expressed by Equation 8. Since all nodes are assumed to be at the same position, the subscript  $n$  used in Equations 4 and 5 is not needed.

$$\hat{\phi}_i = \arg \max_{\phi} \{g_i(\phi)\} \quad (8)$$

The error of interpretation  $i$  is defined by Equation 9. This is the sum of the absolute differences between the DOA estimates of the microphone pairs  $\phi_{n,i}$  and the consensus DOA estimate  $\hat{\phi}_i$ .

$$\phi_{\text{err},i} = \sum_{n=1}^N |\phi_{n,i} - \hat{\phi}_i| \quad (9)$$

### 3.3 Numerical implementation

Since only the position of the peak of the KDE is considered, all factors in Equations 6 and 7 which are independent of  $\phi$  may be ignored. Consequently, the KDE may be simplified as shown in Equation 10. The first and second derivatives are also shown.

$$g_i(\phi|\kappa) = \sum_{n=1}^N \exp(\kappa \cos(\phi - \phi_{n,i})) \quad (10a)$$

$$g_i'(\phi|\kappa) = -\kappa \sum_{n=1}^N \sin(\phi - \phi_{n,i}) \exp(\kappa \cos(\phi - \phi_{n,i})) \quad (10b)$$

$$g_i''(\phi|\kappa) = \kappa \sum_{n=1}^N \exp(\kappa \cos(\phi - \phi_{n,i})) (\kappa \sin^2(\phi - \phi_{n,i}) - \cos(\phi - \phi_{n,i})) \quad (10c)$$

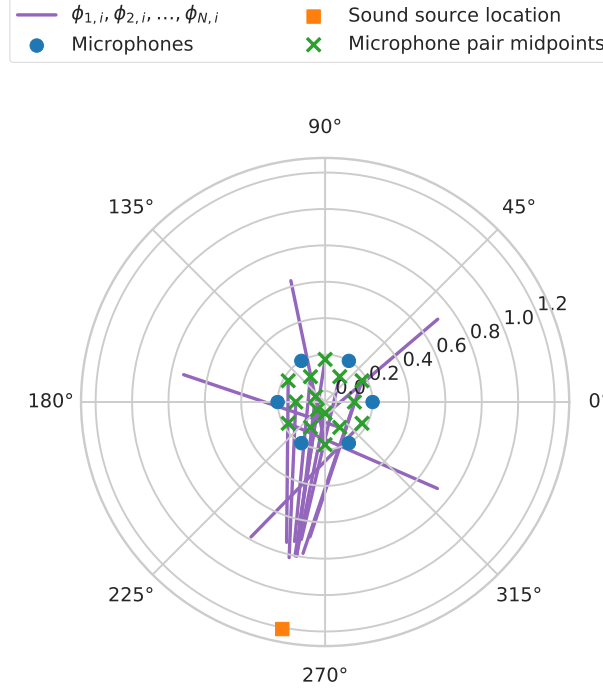


Figure 4: An example of a dataset  $\{\phi_{1,i}, \phi_{2,i}, \dots, \phi_{N,i}\}$  with  $N = 15$  and where 5 of the values are interpreted incorrectly.

The peak of  $g_i(\phi|\kappa)$  may be found using any suitable numerical optimisation function. Since the first and second derivatives are available in closed form and not expensive to calculate, they can be taken advantage of, for example by the Newton Conjugate Gradient (NCG) method [11], which often converges more quickly than other methods.

A different KDE  $g_i(\phi|\kappa)$  is calculated for each of the  $I$  interpretations of  $\{\phi_{1,i}, \phi_{2,i}, \dots, \phi_{N,i}\}$ . The interpretation for which  $\phi_{\text{err},i}$  (Equation 9) is the smallest is regarded as the correct interpretation, and the mode  $\hat{\phi}_i$  (Equation 8) is the final DOA estimate. We will refer to the KDE of the favoured interpretation as  $g_{\text{final}}(\phi|\kappa)$ , where ‘final’ =  $\arg \min_i \{\phi_{\text{err},i}\}$ .

### 3.4 Initialising the optimisation of $g_i(\phi|\kappa)$

While  $g_i(\phi|\kappa)$  may be evaluated directly, a brute-force search for the peak is computationally expensive. This problem is compounded by the fact that there are  $I = 2^N$  interpretations for which the peak of  $g_i(\phi|\kappa)$  must be found. The optimisation may be accelerated considerably by choosing an appropriate starting value for  $\phi$  before applying the NCG method to  $g_i(\phi|\kappa)$ .

To find an appropriate starting value for the optimisation of  $g_i(\phi|\kappa)$ , we calculate an approximation  $\hat{g}_i(\phi|\kappa)$  of  $g_i(\phi|\kappa)$ . Then,  $\arg \max_{\phi} \hat{g}_i(\phi|\kappa)$  is used as the starting point for finding the peak of  $g_i(\phi|\kappa)$ . One strategy for fast estimation of  $g_i(\phi|\kappa)$  is presented here.

A histogram of the values in  $\{\phi_{1,i}, \phi_{2,i}, \dots, \phi_{N,i}\}$  approximates the true distribution as the number of bins increases. Therefore, the convolution of such a histogram with the von Mises kernel approximates  $g_i(\phi|\kappa)$ . An example of a dataset  $\{\phi_{1,i}, \phi_{2,i}, \dots, \phi_{N,i}\}$  is shown in Figure 4, and Figure 5 shows its 8-bin histogram. This histogram may be convolved with the von Mises kernel to obtain the approximation  $\hat{g}_i(\phi|\kappa)$ , after which  $\arg \max_{\phi} \hat{g}_i(\phi|\kappa)$  is used to initialise the NCG optimiser.

The convolution may be implemented using the Fast Fourier Transform (FFT), and the Discrete Fourier Transform (DFT) of the von Mises kernel can be precomputed. This allows  $\hat{g}_i(\phi|\kappa)$  to be computed efficiently. A large number of histogram bins leads to slower calculation of  $\hat{g}_i(\phi|\kappa)$ , but faster optimisation of  $g_i(\phi|\kappa)$ . A smaller number of bins leads to faster calculation of  $\hat{g}_i(\phi|\kappa)$ , but slower optimisation of  $g_i(\phi|\kappa)$ . The best compromise will depend on the exact implementation used and the capabilities of the processors performing the calculations.

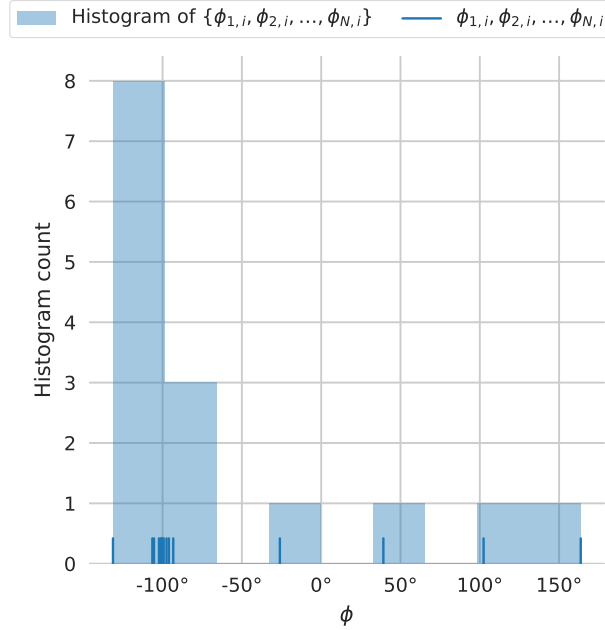


Figure 5: A histogram of the dataset from Figure 4 using 8 bins. The width of each bin is  $45^\circ$ .

The NCG optimisation step may be skipped if speed is valued over accuracy, or if the selected number of histogram bins already places  $\arg \max_{\phi} \hat{g}(\phi | \kappa)$  within the desired accuracy.

## 4 Simulations

The presented algorithm was developed as part of a project which sought to localise elephant rumbles using microphone arrays. Recording devices with circular arrays of 6 omnidirectional microphones with a radius of 20 cm were used (see Figure 6). For this configuration there are  $N = 15$  microphone pairs and  $I = 32768$  possible interpretations of  $\{\phi_1, \phi_2, \dots, \phi_N\}$  to consider per microphone array. One such circular array is used in the following simulation.

The effect of noisy input DOA estimates on the output DOA estimate is also considered in the simulation. The propagation of sound from the SSL to the sensors is not simulated. Therefore, the results are expected to be independent of the SSL, but dependent on the level of noise in the input data.

To initialise the optimisation of  $g_i(\phi | \kappa)$ , the distribution was first approximated by a 512-bin histogram of  $\{\phi_{1,i}, \phi_{2,i}, \dots, \phi_{N,i}\}$  convolved with the von Mises kernel, as suggested in §3.4. This brings the initial value to within  $0.703^\circ$  of the final DOA prediction. Starting from this initialisation, a NCG optimiser locates the peak of  $g_i(\phi | \kappa)$ .

Every iteration of the simulation consists of the following steps:

1. A random SSL is chosen in the annulus defined by  $10\text{m} < r < 1\text{km}$ , where  $r$  is the distance from the origin. The origin is also the midpoint of the circular microphone array.
2. The true DOA from the midpoint of each microphone pair to the sound source is calculated.
3. Gaussian random values with zero mean and a standard deviation of  $\sigma$  are added to the true DOAs, where  $\sigma$  is selected uniformly from  $[0^\circ; 45^\circ)$ . This represents the estimated DOA values from each microphone pair which would constitute the inputs to our algorithm during real-world application.
4. A random value for the concentration  $\kappa$  is chosen uniformly from  $[0.1; 100)$ .
5. Our algorithm is used to estimate a single DOA for the microphone array.
6. The estimated DOA is compared to the true DOA. The algorithm error is defined as the magnitude of the smallest angle between the estimated DOA and the true DOA.

A total of  $10^5$  simulation iterations were performed.

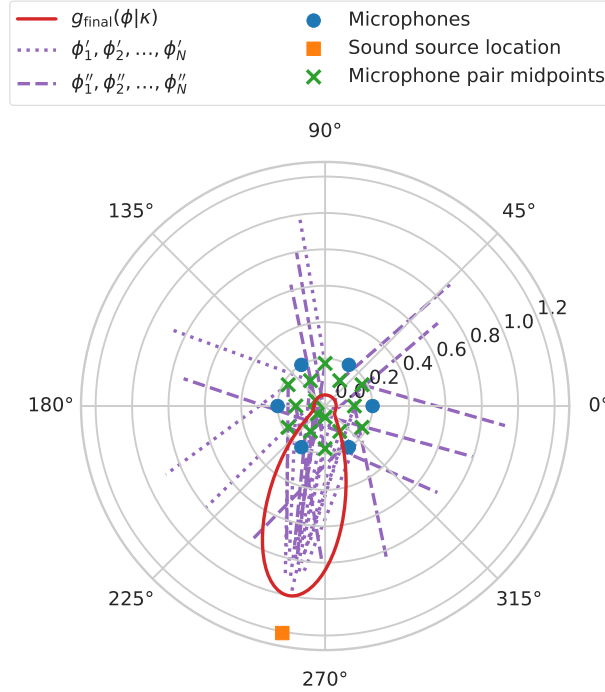


Figure 6: This circular array of 6 microphones, with a radius of 20 cm provides 15 ambiguous DOA estimates. Each ambiguous estimate has one interpretation pointing towards the sound source, and one which is mirrored along the microphone pair axis. The KDE  $g_{\text{final}}(\phi|\kappa)$  yielding the lowest error  $\phi_{\text{err},i}$  is also shown. The mode of this KDE is the DOA estimate provided by our algorithm.

An example of the DOA estimates and the KDE  $g_{\text{final}}(\phi|\kappa)$  of the interpretation yielding the lowest error with this configuration of microphones is shown in Figure 6.

Figure 7 depicts the correlation between the standard deviation of noise in the input data,  $\sigma$ , and the output error. On average, a 3:1 reduction in DOA noise is achieved, indicating that the algorithm is robust against noisy input data.

The polar coordinates of the SSL ( $r; \phi$ ) showed no significant correlation with the dependent variable. The lack of correlation between the value of the SSL coordinates and the output error was to be expected, since the simulation was set up to ensure that the distance between the sound source and the microphone array has no impact on the level of noise in the input data. In practical tests, it is expected that the output error will be affected by the distance to the sound source, since the DOA estimates from the microphone pairs will be less accurate for distant sound sources than for sound sources nearby, causing a positive correlation between the distance to the sound source and the level of noise in the input data.

There was also no discernible correlation between the concentration  $\kappa$  of the von Mises kernel and the dependent variable for the values of  $\kappa$  that were tested. This suggests that  $\kappa$  does not need to be fine-tuned for this algorithm to work properly.

## 5 Practical tests

Tests were performed in a quiet location near Pleateau Road in the Cape Peninsula, South Africa. The ambient noise level at the test site as recorded by our sound recorders is shown in Figure 8. This was done to ensure that the test environment contains only one sound source, with a good signal-to-noise ratio.

Two specially built infrasonic sound recorders with integrated Global Positioning System (GPS) modules were placed 147.7 m apart. Each recorder has a planar array of 6 omni-directional ICS-40300 Microelectromechanical System (MEMS) microphones placed in a circular pattern with 20 cm radius.

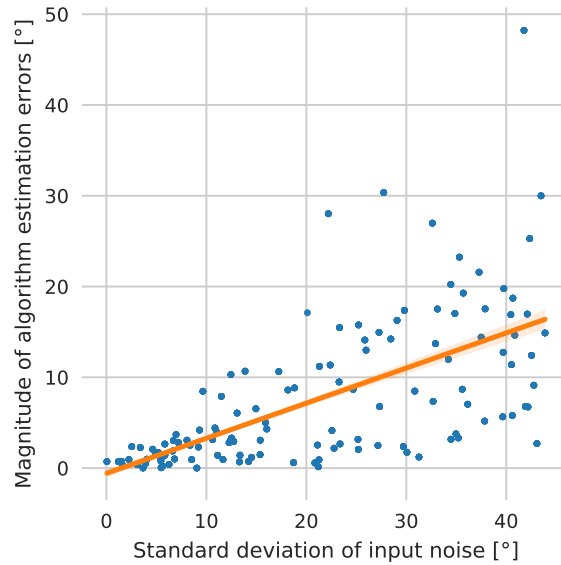


Figure 7: The relationship between the standard deviation of the noise added to the input DOA estimates (step 3 in §4) and the algorithm estimation error (defined in step 6 in §4). Errors in the input data are positively correlated with errors in the estimated DOA, but the latter is on average only a third of the former. Shading around the regression line indicates the 95% confidence intervals. For clean input data, the convolution with the von Mises kernel and the subsequent optimisation introduces some numerical error. In real-world situations, the noise in the input data is expected to be much greater than this numerical noise.

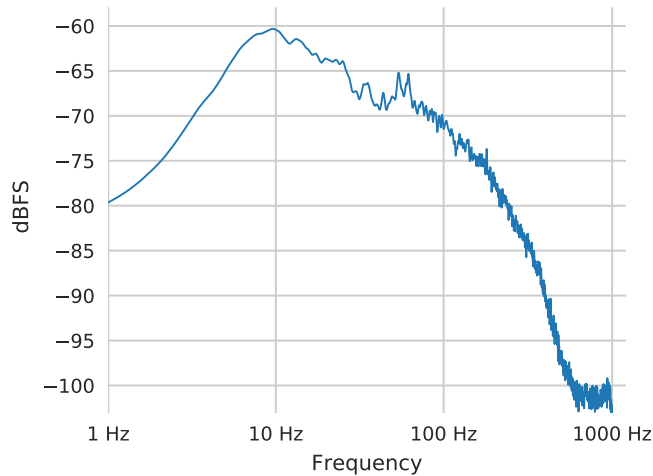


Figure 8: The average magnitude of the ambient noise level at the test site, in dBFS, where 0 dBFS corresponds to the clipping point of the sound recorder’s analog-to-digital converter.



A loudspeaker playing recordings of elephant rumbles and an attached GPS device provided the sound source and SSL ground truth. The loudspeaker and GPS device were carried along a meandering path between the recording devices for about 4 minutes.

The incoming audio was split into overlapping frames of 1 s each, with a frame skip of 200 ms. For each frame, TDOAs between the microphone pairs were estimated using cross correlation and the DOA for each microphone pair was calculated using Equation 1. The algorithm proposed in §3 was used with 512 histogram bins and a kernel concentration of  $\kappa = 10$  to estimate the DOA of the sound source with respect to the microphone array for each window.

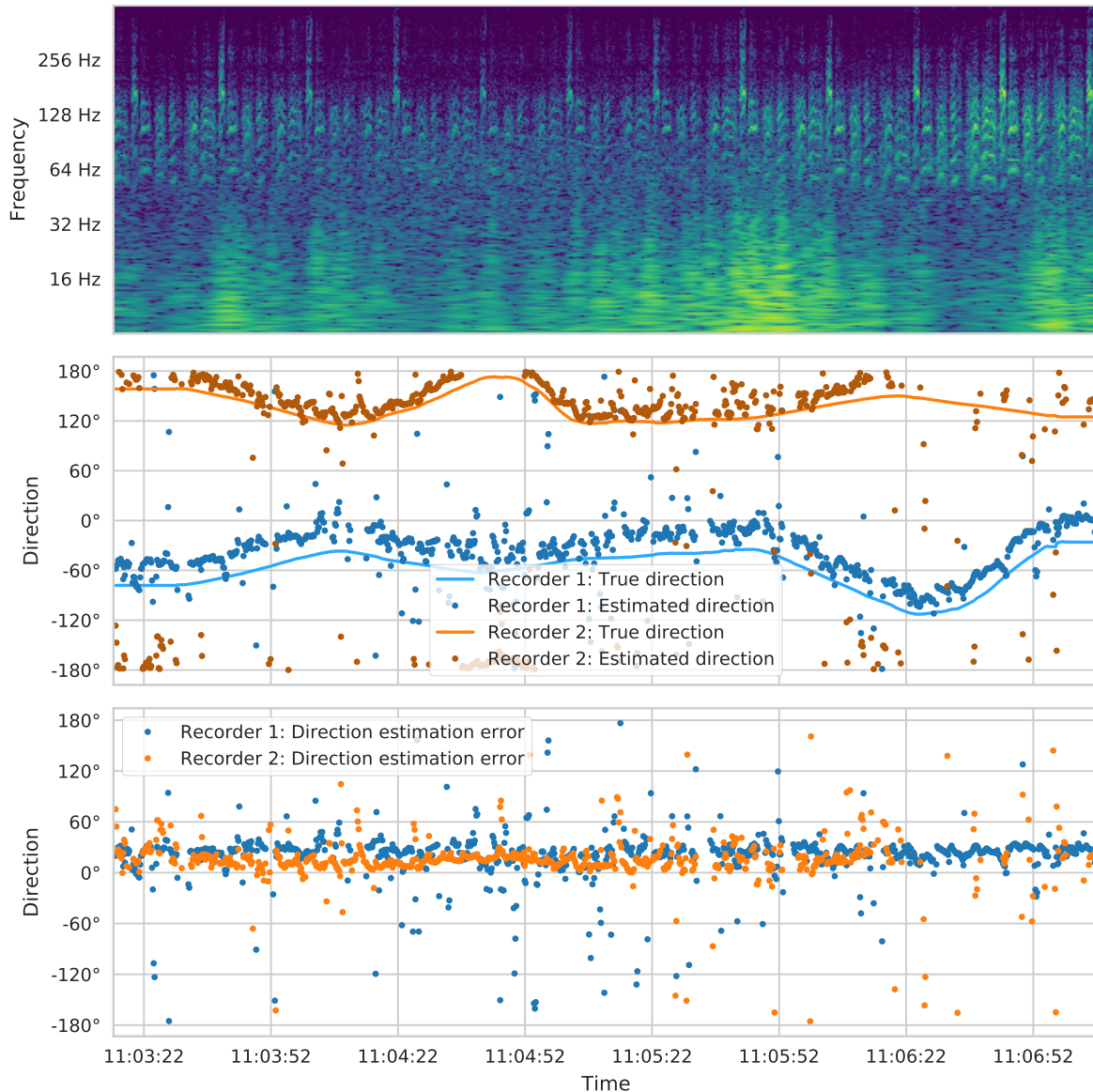


Figure 9: From top to bottom: 1. The spectrogram of the recording, 2. the true DOA (lines) and estimated DOA (dots) of the sound sources, and 3. the errors in the DOA estimates. The time axis is shared.

Figure 9 shows, from top to bottom: 1. The spectrogram of the recording, 2. the true (lines) and estimated (dots) DOA of the sound sources, and 3. the errors in the DOA estimates. The time axis is shared. The repeated harmonic patterns seen in the 40 Hz to 256 Hz band are the reproduced elephant rumbles. Some unwanted low-frequency noise can be seen in the 8 Hz to 32 Hz band, especially at 11:05:52. The estimated directions deviate from the true directions (calculated using the GPS coordinates) by a constant value, but in general follow the SSL faithfully.

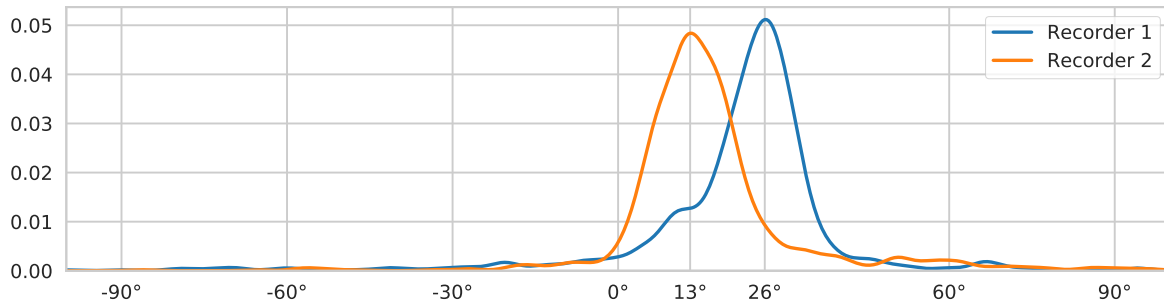


Figure 10: Estimation of the distribution of DOA errors for each recorder. The mode (position of the peak) of each distribution is probably equal to the orientation error of the recorder, since each recorder was placed and oriented manually. In practice, the DOA estimates may be improved by subtracting the mode. Recorders 1 and 2 provided estimates with standard deviations of  $20.4^\circ$  and  $15.2^\circ$ , respectively.

With multiple recorders, these DOA estimates may be used to estimate the SSL as shown in §2.2, and techniques like Kalman filtering or Probability Hypothesis Density (PHD) filtering may be used to combine these estimates into a single track [12].

Figure 10 shows the estimated distribution of DOA errors for each recorder. The standard deviations of these distributions quantify the accuracy of our DOA estimates. They are  $20.4^\circ$  and  $15.2^\circ$ , respectively.

The non-zero modes of these errors might be ascribed to the inaccurate manual orientation of the devices during testing. In practice, such errors may be corrected by adding a constant angle to all DOA estimates before triangulation or by aligning the devices accurately using laser pointers.

## 6 CONCLUSION

A method of obtaining an unambiguous DOA estimate from a non-linear, planar microphone array was presented. All  $2^N$  possible interpretations of the ambiguous DOA estimates from all  $\binom{M}{2}$  possible microphone pairs within the  $M$ -element array were considered. For every interpretation, the consensus DOA estimate was deduced from the mode of the KDE of all DOA estimates from the  $N$  microphone pairs. The DOA consensus estimate with the lowest average absolute deviation from the DOA estimates obtained from the  $N$  microphone pairs was chosen as the final DOA, thereby eliminating the ambiguities that existed in the input data. Efficient numerical implementation of the algorithm using the FFT is possible. Simulations showed a 3:1 reduction in input noise, and practical outdoor tests with two real sound recorders provided DOA estimates with standard deviations of  $20.4^\circ$  and  $15.2^\circ$ , respectively.

## References

- [1] C. Proukakis and A. Manikas, “Study of ambiguities of linear arrays,” in *Acoustics, Speech, and Signal Processing, 1994. ICASSP-94., 1994 IEEE International Conference on*, vol. 4. IEEE, 1994, pp. IV–549.
- [2] G. Ottoy and L. De Strycker, “An improved 2d triangulation algorithm for use with linear arrays,” *IEEE Sensors Journal*, vol. 16, no. 23, pp. 8238–8243, 2016.
- [3] P. Dostálek, V. Vašek, and J. Dolinay, “Direction of sound wave arrival determination using time-delay estimation and beamforming methods,” *WSEAS Transactions on Circuits and Systems*, 2009.
- [4] I. J. Tashev, *Sound capture and processing: practical approaches*. John Wiley & Sons, 2009.
- [5] R. I. Hartley and P. Sturm, “Triangulation,” *Computer vision and image understanding*, vol. 68, no. 2, pp. 146–157, 1997.
- [6] S. M. Stigler, “Gauss and the invention of least squares,” *The Annals of Statistics*, pp. 465–474, 1981.
- [7] W. A. Fuller, *Measurement error models*. John Wiley & Sons, 2009, vol. 305.
- [8] R. VON MISES, “Über die ‘ganzzahligkeit’ der atomgewicht und verwandte fragen.” *Phys. Z.*, vol. 19, pp. 490–500, 1918.
- [9] K. V. Mardia, *Statistics of directional data*, ser. Probability and mathematical statistics: a series of monographs and textbooks. London: Academic Press, 1972.

- [10] —, “Statistics of directional data,” *Journal of the Royal Statistical Society. Series B (Methodological)*, pp. 349–393, 1975.
- [11] J. Nocedal and S. J. Wright, *Numerical optimization*, 2nd ed., ser. Springer series in operations research. New York: Springer, 2006.
- [12] A. J. Hunter, L. Fillinger, M. Zampolli, and M. C. Clarijs, “Data fusion from multiple passive sonar nodes for target localisation and false alarm reduction,” in *11th European Conference on Underwater Acoustics 2012, ECUA 2012, 2-6 July 2012, Edinburgh, PART 3, 34 1, 577-584*, 2012.